Chapter 7
Microautoradiography (MAR)

Keywords Microautoradiography · Microautoradiography method improvement · ^{109}Cd · ^{33}P · ^{137}Cd · Microscopic distribution · Rice · Grain

7.1 MAR Method Developed

Microautoradiography (MAR) is a conventional imaging method based on the daguerreotype that was used to take photographs several decades ago. This technique was applied to visualize the distribution of radionuclide-labeled compounds within a tissue section. Although the distribution of radionuclides could be visualized in greater detail by MAR than by the IP (imaging plate) method because of the high resolution of MAR, IP imaging has become a widely used method because it has greater quantitative ability and sensitivity than MAR. For these reasons, MAR was performed only to obtain finer images and higher resolution of the radionuclide distribution. However, the application of the classical MAR method to plant tissue sections is associated with several difficulties, such as the preparation of thin sections. To overcome these difficulties, we developed a MAR method for imaging plant tissue section cells [1, 2, 3]. This method was applicable to fresh-frozen plant tissue and has two distinct features: (1) the sample was kept frozen from collected tissue for radioisotope detection, making it possible to fix solutes without solvent exchange, and (2) a 1.2 μm thick polyphenylene sulfide film was inserted between the fresh-frozen plant section and the photosensitive nuclear emulsion to keep the section separated from the emulsion before autoradiography was conducted, which significantly improved the quality of the section until microscopic detection, the quality of the MAR image, and the success rate.

There are two types of photosensitive nuclear emulsion preparations in MAR. In one, the photosensitive nuclear emulsion coats the plant section set on the slide to create a slide–section–emulsion layer. However, in this case, coated plant surfaces frequently exhibit irregularity due to the structure of plant tissue and produce a mixture of silver grains and plant tissue in the same microscope field. In our initial procedure, we attempted to improve this type of MAR in terms of overcoming the irregularity by optimizing the microscope manipulation, e.g. the composition of the

T. M. Nakanishi, *Novel Plant Imaging and Analysis*,
https://doi.org/10.1007/978-981-33-4992-6_7

microscope images sequentially obtained moving in the z-axial direction. However, the shadow of the plant cells and silver grains were not clearly distinguished, and the quality of the MAR images obtained thus far was insufficient for practical use.

In other preparation, the sliced section was mounted on photosensitive nuclear emulsion pasted on a glass surface, presenting a slide–emulsion–section layer and rarely resulting in irregularity. However, this type of MAR method had other problems, principally related to retention of the section during the development process of the emulsion film. In addition, the adhesive film for retaining the fresh-frozen section was found to hamper the autoradiographic procedure. In fact, we also attempted to develop an autoradiograph after the adhesive film was stripped from the sliced section sample while the sliced section remained on the emulsion surface. After several trials, the success rate of sample retention during the development process was found to be insufficient for routine usage.

The new method we developed achieved clear separation of the photosensitive nuclear emulsion and the section after exposure by sandwiching a 1.2 μm thick film between them (Fig. 7.1).

The emulsion on the glass slide and the section on the adhesive film were individually processed to develop the autoradiograph and tissue image, respectively. This procedure achieved high-quality image acquisition of the tissue section because the tissue section was rescued before the glass slide was exposed to the reagent for the development process. Other advantages of this method are an extremely high rate of sample retention and a wide choice of tissue staining. On the other hand, the disadvantage of this method is that the positioning accuracy could be reduced due to the separation of the section and the photosensitive nuclear emulsion. The insertion of the 1.2 μm thick film created a concern about the masking effect, particularly in detecting very low-energy β-rays. To address this point, a trial experiment was performed using ^{3}H, which emits β particles with a mean energy of only 5.7 keV, and obtained evidence that the β-ray could produce silver grains through the film (data not shown).

7.2 MAR of ^{109}Cd and ^{33}P in a Rice Plant

As an example of MAR images, the ^{109}Cd distribution of nonelongated stems and shoots above the stem of a rice plant was selected. The distribution images of ^{109}Cd and ^{33}P in the cross section of the crown root are shown.

Figure 7.2 shows the distribution of ^{109}Cd in the rice shoot after 24 h of ^{109}Cd absorption. When the light image and MAR image were superimposed, the xylem cells (Xy) were found to contain less ^{109}Cd. ^{109}Cd was more concentrated in the nodal vascular anastomoses (NVA) and the regular vascular bundles (Rv) than in the enlarged vascular bundles (Ev). The ^{109}Cd concentration in phloem cells was found to be particularly high, whereas the xylem cells contained only small amounts of ^{109}Cd. In the leaf sheath, the large vascular bundles produced more silver grains than the small vascular bundles. The ^{109}Cd MAR image could first provide evidence of

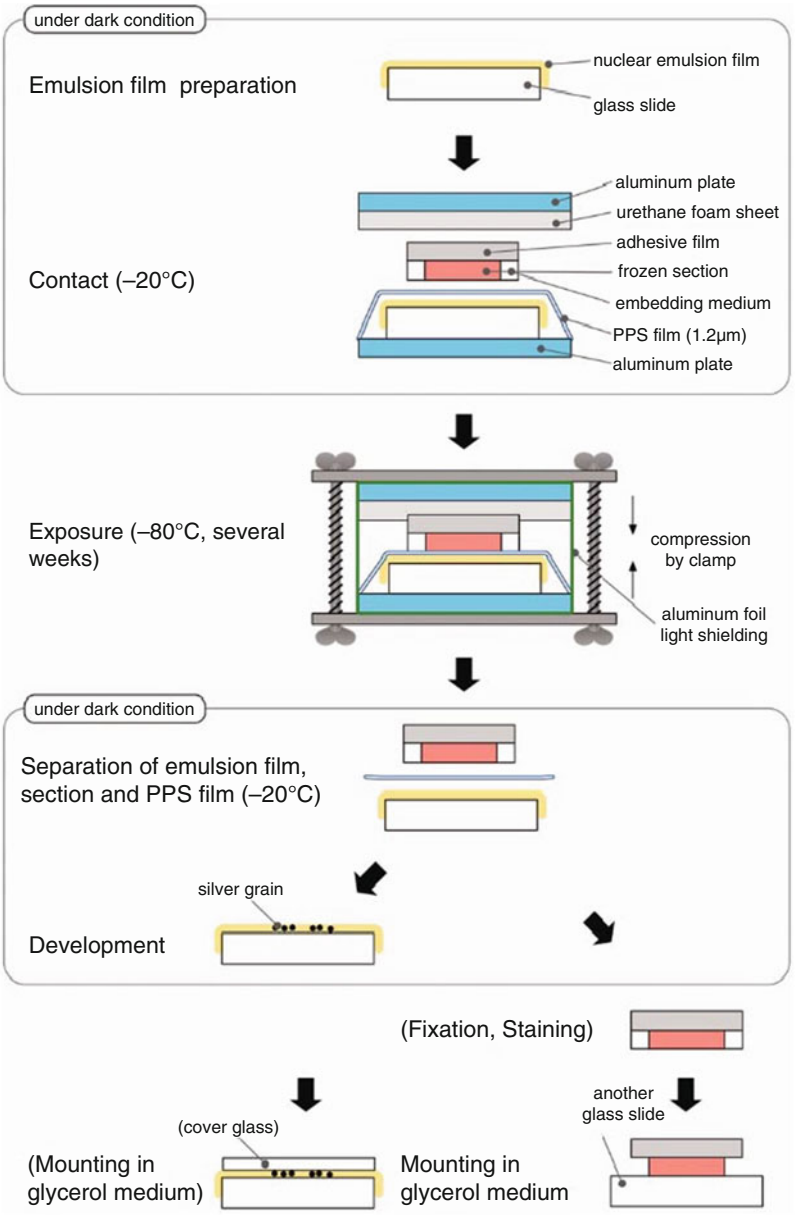

Fig. 7.1 Schematic illustration of the revised microautoradiography (MAR) method for fresh-frozen plant sections characterized by the separation process [1]. A 1.2-μm-thick polyphenylene sulfide (PPS) film was inserted between the frozen section sample and the photosensitive nuclear emulsion on the glass slide to easily separate the section and emulsion after several weeks of exposure. Progression of the development and tissue processing separately improved the likelihood of success of MAR, and fresh-frozen plant sections of 5 μm in thickness attached to the adhesive film were prepared

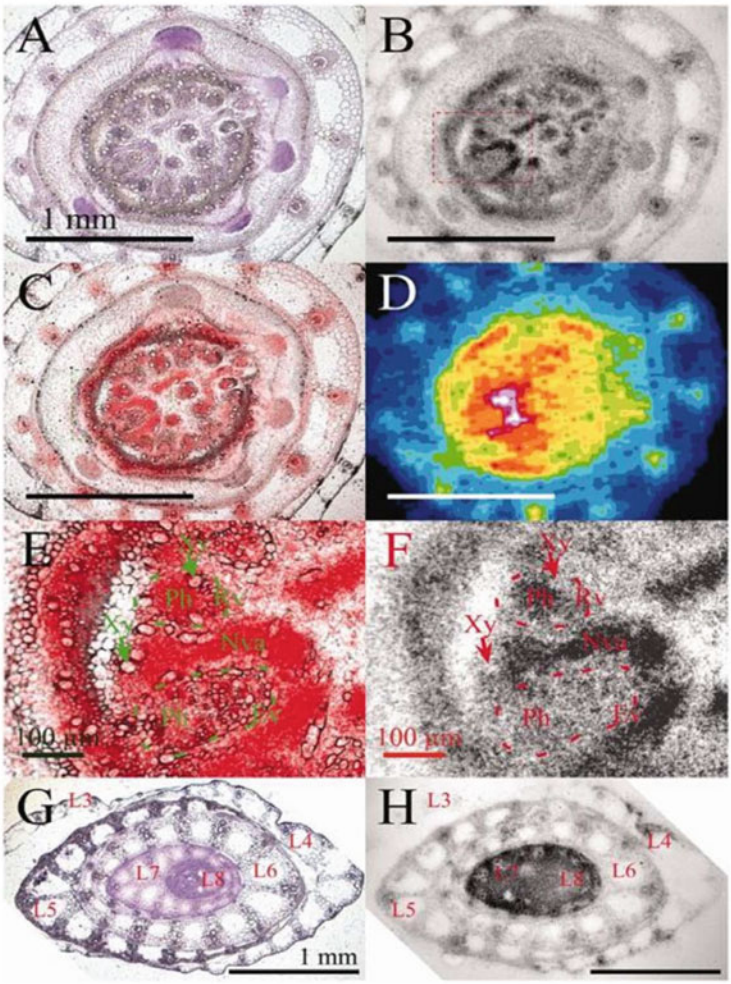

Fig. 7.2 Distribution of ^{109}Cd in rice, nonelongated stem and shoot above the stem [1]. (**a**) Transverse section of the nonelongated stem including the node stained with hematoxylin. (**b**) Autoradiograph of (**a**) showing the localization of ^{109}Cd. (**c**) Superimposed image of (**a**) and (**b**) after the RGB color in (**a**) was converted to grayscale and the *black color* in (**b**) was converted to *red*. (**d**) IP image of (**a**) with pseudocolor. (**e**, **f**) Magnified images of the node tissue corresponding to the open boxes in (**c**) and (**b**). (**g**) Transverse section of the part of the shoot above the stem stained with hematoxylin. The leaves were numbered according to their growth from L3 (old) to L8 (young). The first and second leaves (L1 and L2) were in senescence and depressed. (H) Autoradiograph of (G) of the ^{109}Cd accumulation in the young growing sink leaves, e.g. the seventh (L7) and eighth leaves (L8). Xy: xylem cells; NVA: nodal vascular anastomoses; Rv: regular vascular bundles; Ev: enlarged vascular bundles; Ph: phloem. The radioactivity of ^{109}Cd in the phloem (Ph) in the Rv was significantly higher than that in the Ev

the intensive accumulation of ^{109}Cd in the phloem in the nonelongated stem as early as 24 h after ^{109}Cd administration to the root. The xylem to phloem transport system mediating ^{109}Cd transport to the phloem in the nonelongated stem implied a significant impact on cadmium partitioning in rice plants.

With regard to the ^{109}Cd signals detected in these tissues using an IP, the signal intensity had a linear relationship with radioactivity. Although the MAR images were related to the ^{109}Cd concentrations, there was no linear relationship between the whiteness of the image and the ^{109}Cd amount, since there were sigmoidal dose–response curves, which are the principle of daguerreotype images. Another problem was that it was difficult to compare the blackening quantitatively across slides, since the precise thickness of the emulsion layer formed on the glass slide could differ among slides. When the stripping film with a uniform thickness was commercially available, the quantitative capability of MAR was ensured; however, the film is no longer in production. Therefore, the precise quantitative capability of MAR is now difficult to ensure.

Figures 7.3 and 7.4 show the distribution of ^{109}Cd and ^{33}P in the crown root of rice plants after 24 h and 15 min of absorption, with two and four metaxylem cells in the middle, respectively. As shown in Fig. 7.3, the ^{109}Cd signal intensity was low in the cortex tissue inside the sclerenchymatous (S) cell layer. A high silver grain image was observed at the outer circle overlapping with the epidermis, exodermis, and sclerenchyma cells, whereas the cortex tissue contained a small amount of ^{109}Cd, which was also observed in the IP image. Within the xylem cells in the stele, which had a high concentration of ^{109}Cd, the degree of blackening was similar to that in the surrounding cells, which could not be distinguished by the IP image. MAR clearly revealed the distribution of ^{109}Cd at the tissue level with high resolution.

Figure 7.4 shows the distribution of ^{33}P in the crown roots of rice plants after 15 min of absorption. Interestingly, ^{33}P-phosphate produced many silver grains on the sclerenchyma cells and their neighboring cells in the cortex, adjacent to the epidermis and exodermis cells, indicating that phosphate could easily pass through the epidermis and exodermis cell layers. Phosphate remained in the area of the sclerenchyma cells, which were expected to be connected with each other by Casparian strips, and then easily reached the stele without accumulating in the cortex. The success in visualizing ^{33}P after 15 min of exposure demonstrated both the characteristic transport mechanism of phosphate within the root tissue and the high sensitivity of autoradiography, suggesting the high potential applicability of MAR for ion uptake and transport analysis.

7.3 MAR of ^{137}Cs in a Rice Grain

The 3D ^{137}Cs image in a rice grain was shown in the previous chapter (Figs. 6.3 and 6.5), where ^{137}Cs accumulated in the embryo and the outer bran layer. To acquire a finer image of ^{137}Cs distribution in the grain, especially in the embryo, MAR was performed on rice grain containing ^{137}Cs. A rice plant was supplied with ^{137}Cs

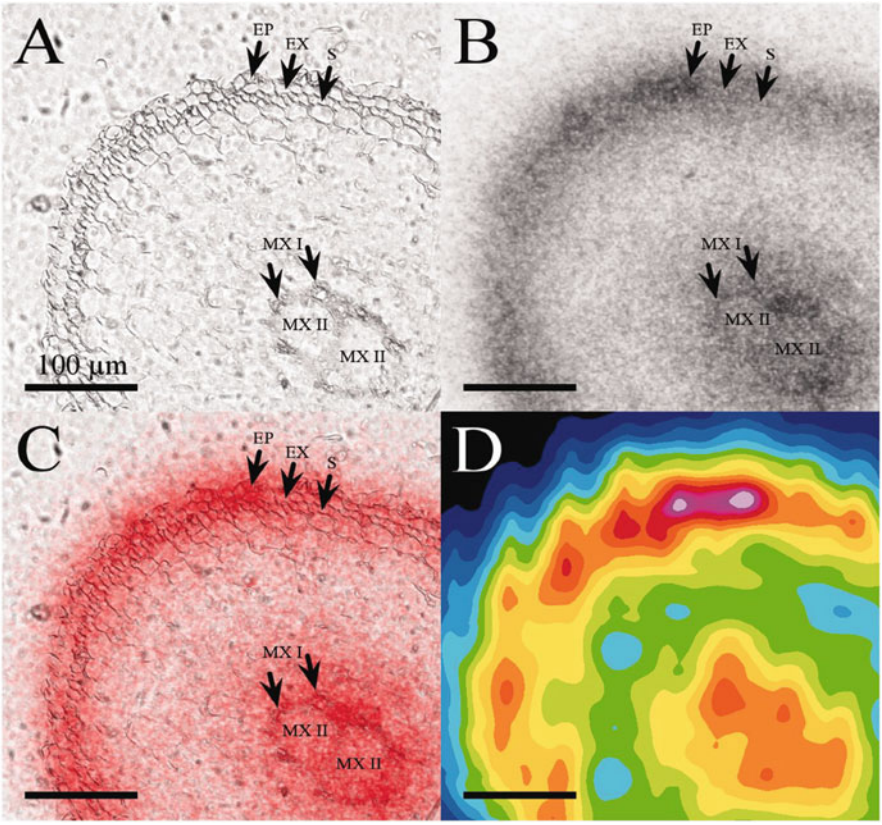

Fig. 7.3 Distribution of ^{109}Cd in the rice crown root after 24 h of ^{109}Cd absorption [1]. (**a**) Transverse section of the root with two metaxylem II (MX II) cells in the middle. (**b**) MAR of (**a**). (**c**) Autoradiograph superposed to (**a**). Red color was added. (**d**) IP image of the section adjacent to (**a**). Pseudocolor was added. The ^{109}Cd signal intensity was low in the cortex tissue inside the S cell layer. Arrows denote the root epidermis (EP), exodermis (EX), sclerenchymatous (S) cell layers, and metaxylem I and II (MX I and MX II) cells. The arrows denote the same site as Fig. 7.4. The ^{109}Cd signal intensity was low in the cortex tissue inside the S cell layer

solution (200 Bq/mL) for 24 h when flowering was started. Then, after 28 days, the mature brown rice was harvested, and MAR images were acquired. Figure 7.5 shows the distribution of ^{137}Cs in the embryo. As shown in the figure, most ^{137}Cs accumulated in the scutellum, and a very small amount of ^{137}Cs was observed in the plumule, radicle, and embryonic root, suggesting that the tissue with meristems that grew after germination was highly protected from the heavy element Cs.

To compare the distribution of Cs with those of the other elements in the embryo of brown rice, SEM/EDS (scanning electron microscopy/energy dispersive X-ray spectroscopy) was performed to acquire the distributions of K, Mg, N, P, Si, and Ca. As shown in the figure, K, Mg, and P showed higher concentrations at the

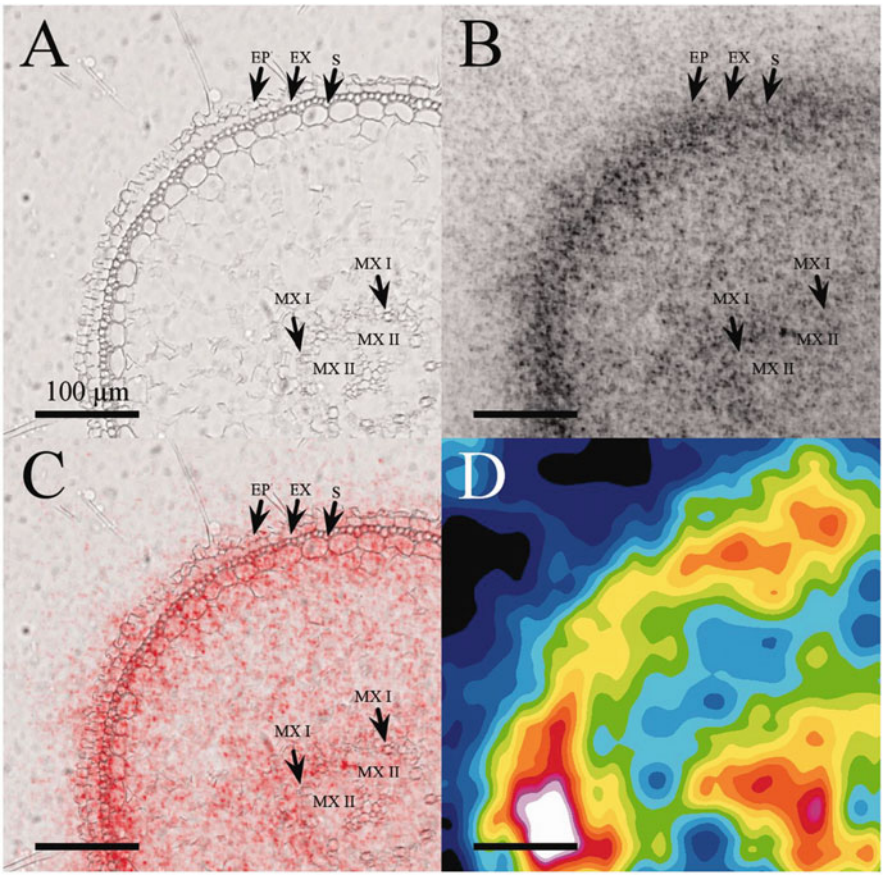

Fig. 7.4 Distribution of ^{33}P in the rice crown root after 15 minutes of ^{33}P-phosphate absorption [1]. (**a**) Transverse section of the root with four metaxylem II (MX II) cells in the middle. (**b**) Autoradiograph superposed to (**a**). Red color was added. (**c**) IP image of (**a**). Pseudocolor was added. The *arrows* denote the same site as Fig. 7.3. ^{33}P-phosphate concentrated in the sclerenchyma cells and their neighboring cells in the cortex, which were adjacent to the epidermis and exodermis cells

embryo; however, similar to ^{137}Cs, these elements were also concentrated at the scutellum, not at the plumule or radicle.

Since ^{137}Cs behavior in rice plants has attracted attention, especially after the Fukushima nuclear accident, the uptake behavior of ^{137}Cs was studied in comparison with that of K. The differences in the transport characteristics in plants between potassium (K^+) and cesium (Cs^+) were investigated using their radionuclides $^{42}K^+$ and $^{137}Cs^+$. The result is briefly introduced below. A tracer experiment using nutrient solutions supplied with ^{42}K and ^{137}Cs revealed that the ratio of the root's K^+ uptake rate to its Cs^+ uptake rate was 7–11 times higher than the K^+ to Cs^+ concentration ratio in the solution, and the number varied depending on the K concentration in the

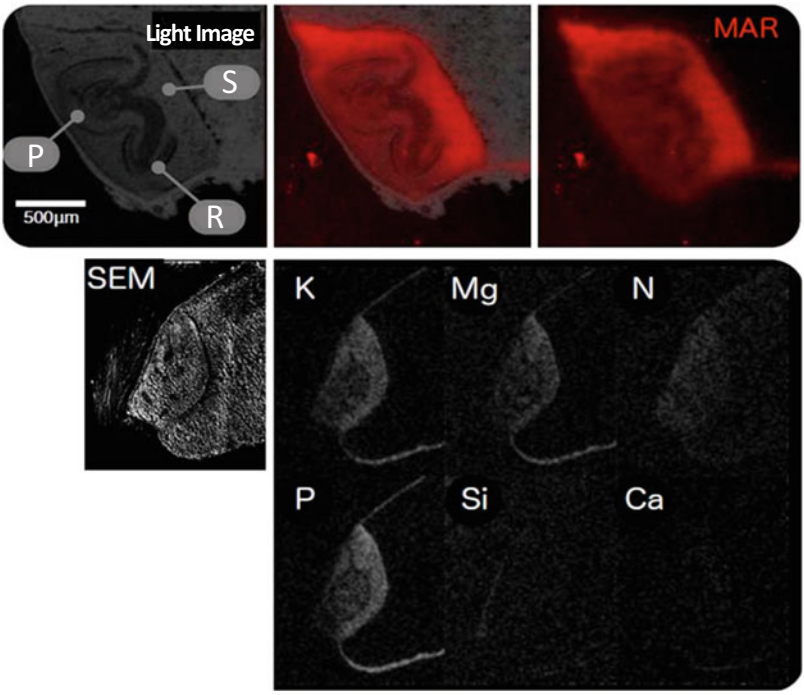

Fig. 7.5 Distribution of ^{137}Cs in the embryo of a rice train partially. *Red color* was added to the microautoradiography image (MAR) according to the intensity of the image. In the light image under the microscope, P: plumule, S: scutellum, R: radicle (embryonic root). The distributions of K, Mg, N, P, Si, and Ca are shown in grayscale. K, Mg, and P concentrations were high in the embryo; however, they were not accumulated in the plumule or radicle, which is similar to those of ^{137}Cs

solution as well as on the growth condition. After entering through the root tissues, the $^{42}K^+$ to $^{137}Cs^+$ ratio in the shoots was 4.3 times higher than the value in the roots. However, the $^{42}K^+$ to $^{137}Cs^+$ ratio in each leaf did not differ significantly, indicating that the primary transport of K^+ and Cs^+ in the shoots is similarly regulated. In contrast, among the radionuclides stored in the roots over 4 h, 30% of the $^{42}K^+$ was transferred from the roots over the following hour, whereas only 8% of $^{137}Cs^+$ was moved. In addition, within the xylem, K^+ was shown to travel slowly, whereas Cs^+ passed quickly through the roots into the shoots. Our study demonstrated the very different transport patterns for the two ions in the root tissue, employing $^{42}K^+$ and $^{137}Cs^+$.

Bibliography

1. Hirose A, Kobayashi NI, Tanoi K, Nakanishi TM (2014) A Microautoradiographic Method for Fresh-Frozen Sections to Reveal the Distribution of Radionuclides at the Cellular Level in Plants. Plant and Cell Physiology 55:1194–1202
2. Sugita R, Hirose A, Kobayashi NI, Tanoi K, Nakanishi TM (2016) Imaging techniques for radiocesium in soil and plants. In: Agricultural Implications of Fukushima Nuclear Accident. Nakanishi, T.M., Tanoi, K, pp 247–263
3. Hirose A (2013) Ph.D. thesis. In: The University of Tokyo